An Effective Method for Detecting Double JPEG Compression With the Same Quantization Matrix

Jianquan Yang, Jin Xie, Guopu Zhu, *Senior Member, IEEE*,
Sam Kwong, *Fellow, IEEE*, and Yun-Qing Shi, *Fellow, IEEE*

***Abstract*— Detection of double JPEG compression plays an important role in digital image forensics. Some successful approaches have been proposed to detect double JPEG compression when the primary and secondary compressions have different quantization matrices. However, detecting double JPEG compression with the same quantization matrix is still a challenging problem. In this paper, an effective error-based statistical feature extraction scheme is presented to solve this problem. First, a given JPEG file is decompressed to form a reconstructed image. An error image is obtained by computing the differences between the inverse discrete cosine transform coefficients and pixel values in the reconstructed image. Two classes of blocks in the error image, namely, rounding error block and truncation error block, are analyzed. Then, a set of features is proposed to characterize the statistical differences of the error blocks between single and double JPEG compressions. Finally, the support vector machine classifier is employed to identify whether a given JPEG image is doubly compressed or not. Experimental results on three image databases with various quality factors have demonstrated that the proposed method can significantly outperform the state-of-the-art method.**

***Index Terms*— Digital forensics, double JPEG compression, rounding error, truncation error.**

I. Introduction

With the development of image processing technology in the past decades, digital image tampering becomes much easier without leaving obvious visual traces. It is well known that JPEG, as an image compression standard [1], is widely applied in digital cameras and image processing softwares. Hence, the JPEG related forensic issues [2]–[7] have been receiving more and more attention recently. Some research works [8]–[13] have been proposed for detecting double JPEG compression due to it is often involved in some forensic scenarios with respect to tampering JPEG images. For example, in the scenario of image splicing, assuming that a region from a source JPEG image is copied to the target image and the resulting composite image is JPEG recompressed, the presence of splicing can be revealed by detecting double JPEG compression region by region in the composite image. In addition, some steganographic schemes such as F5 [14] and OutGuess [15] can generate doubly compressed images if the input cover image is originally in JPEG format. So detection of double JPEG compression is also helpful to the development of sophisticated steganalytic algorithms [12].

According to whether the grids of block-wise discrete cosine transform (DCT) between the primary and the secondary JPEG compressions are aligned or not, double JPEG compression can be categorized into two classes: one is aligned double JPEG compression [8]–[13], [16], [17], the other is non-aligned double JPEG compression [18]–[21]. As for aligned double JPEG compression, according to whether the quantization matrices of the primary and secondary compressions are identical or not, it can be further categorized into two subclasses, i.e., aligned double JPEG compression with different quantization matrices [8]–[13] and that with the same quantization matrix [16], [17]. For detecting aligned double JPEG compression with different quantization matrices, some successful methods have been proposed. Lukáš and Fridrich [8] proposed to detect doubly compressed images by exploring the statistical artifacts called "double peaks" or "missing values" in the histogram of JPEG coefficients (i.e., quantized discrete cosine transform coefficients) from individual modes. Popescu and Farid [9] proposed to measure the underlying periodic artifacts of JPEG coefficient histograms via Fourier transform for detection of double JPEG compression. In [10], Fu *et al.* found that the distribution of the first digits of JPEG alternating-current (AC) coefficients follows a generalized Benford's law, which can be used to distinguish between singly and doubly JPEG compressed images. Moreover, in [11], by applying the generalized Benford's law to some specially selected individual AC modes, the performance of detecting double JPEG compression can be further improved. Benford's law is also used to estimate the number of JPEG compressions [22]. In [12], Pevný and Fridrich proposed to use histogram pattern of low-frequency JPEG coefficients

Manuscript received April 4, 2014; revised July 23, 2014; accepted September 9, 2014. Date of publication September 19, 2014; date of current version October 9, 2014. This work was supported in part by the National Natural Science Foundation of China under Grant 61003297, Grant U1135001, and Grant 61202415, in part by the Natural Science Foundation of Guangdong Province under Grant S2013010011806, in part by the Shenzhen Peacock Program under Grant KQCX20120816160011790, and in part by the Knowledge Innovation Program of Shenzhen under Grant JCYJ20130401170306848. The associate editor coordinating the review of this manuscript and approving it for publication was Prof. Chiou-Ting Hsu. *(Jianquan Yang and Jin Xie contributed equally to this work.)*

J. Yang and G. Zhu are with the Shenzhen Institutes of Advanced Technology, Chinese Academy of Sciences, Shenzhen 518055, China (e-mail: jq.yang@siat.ac.cn; guopu.zhu@gmail.com).

J. Xie was with the Shenzhen Institutes of Advanced Technology, Chinese Academy of Sciences, Shenzhen 518055, China. He is now with New York University at Abu Dhabi, Abu Dhabi, United Arab Emirates (e-mail: jin.xie@siat.ac.cn).

S. Kwong is with the Department of Computer Science, City University of Hong Kong, Hong Kong (e-mail: cssamk@cityu.edu.hk).

Y.-Q. Shi is with the Department of Electrical and Computer Engineering, New Jersey Institute of Technology, Newark, NJ 07102 USA (e-mail: shi@njit.edu).

Color versions of one or more of the figures in this paper are available online at http://ieeexplore.ieee.org.

Digital Object Identifier 10.1109/TIFS.2014.2359368

as features to classify singly and doubly JPEG compressed images. Alternatively, Chen *et al.* [13] utilized the transition probability matrices derived from the differential JPEG 2-D arrays along various directions to reveal the presence of JPEG recompression.

For detecting aligned double JPEG compression with the same quantization matrix, however, the above-mentioned methods [8]–[13], which are originally not designed for this scenario, fail to achieve satisfactory performance, because they cannot effectively characterize the minor artifacts caused by JPEG recompression with the same quantization matrix. Huang *et al.* [16] first addressed this issue by proposing a novel perturbing-thresholding method. They found that when a JPEG image is compressed over and over again the number of different JPEG coefficients[1] between the sequential two versions will monotonically decrease. Based on this observation, single and double JPEG compressions can be distinguished by comparing the number of different JPEG coefficients with an image-dependent threshold. The threshold is obtained by using a random perturbing strategy. That is, a portion of JPEG coefficients from the given JPEG image are first randomly selected, and then modified by adding 1 or subtracting 1 arbitrarily. Then, the modified JPEG image is recompressed with the same quantization matrix, and a value is obtained by counting the different JPEG coefficients between the given JPEG image and its recompressed version. The above procedure is repeated multiple times and the resulting values are averaged to be the threshold. In their method, how to determine the ratio of JPEG coefficients to be perturbed is a crucial step, and the authors proposed to obtain the proper ratio through a try-and-error procedure. Recently, Lai and Böhme [17] studied the properties of block convergence during the repeated JPEG compressions with quality factor 100 (JPEG-100). Then, based on the analysis of block convergence, the authors presented forensic methods to detect JPEG-100 compression in grayscale bitmaps, to estimate the times of JPEG-100 compressions, to identify the DCT implementation, and further to reveal image tampering. Note that, for abbreviation, double (JPEG) compression refers to aligned double JPEG compression with the same quantization matrix hereinafter, unless otherwise specified.

Rather different from the method reported in [16], in this paper we present another effective method that utilizes error-based statistical features (EBSF). Firstly, an error image is formed by computing the differences between the inverse DCT (IDCT) coefficients (i.e., the float values before being rounded/truncated to the range $[0, 255]$) and pixel values during JPEG decompression. Two classes of error blocks in the error image are defined, i.e., rounding and truncation error blocks. Subsequently, statistical differences of the rounding and truncation error blocks between single and double JPEG compressions are characterized by three subsets of features in both the spatial and DCT domains. Finally, under the machine learning framework, the extracted features are combined to detect double JPEG compression with the same quantization matrix. Extensive experiments have been conducted to evaluate the effectiveness of the proposed EBSF method, and the results have demonstrated that it remarkably outperforms the state-of-the-art method [16].

The rest of this paper is organized as follows. In Section II, we briefly review the error in JPEG compression and decompression. Section III presents in detail the proposed method, which mainly includes the analysis of error blocks in JPEG compression, and feature extraction for detecting double JPEG compression. The experimental results on three representative image databases are reported and discussed in Section IV. Section V concludes the paper.

II. Error in JPEG Compression and Decompression

There are three major steps in JPEG compression: discrete cosine transform of 8×8 image blocks, quantization of DCT coefficients, and entropy encoding of the quantized DCT coefficients. JPEG decompression is performed in the reverse order: entropy decoding, de-quantization and inverse DCT. There exist three kinds of error during JPEG compression and decompression. The first kind of error is called the quantization error, which occurs in the process of JPEG compression. It is defined as the difference between the float value of the divided DCT coefficient before rounding and its nearest integer value (i.e., the aforementioned JPEG coefficient) [16].

Both the second and third kinds of error exist in the process of JPEG decompression. After performing IDCT on the de-quantized JPEG coefficients, the resulting IDCT coefficients which are float values should be rounded to their nearest integers, and truncation is even needed if the rounded IDCT coefficients exceed the range [0, 255]. Accordingly, the difference between the float IDCT coefficient and its rounded integer is called the rounding error (note that it occurs only when the rounded IDCT coefficient falls in the range of [0, 255]); while the difference between the float IDCT coefficient and its truncated integer (i.e., 0 or 255) is called the truncation error.

It is worth noting that the float un-quantized DCT coefficient cannot be obtained, so the quantization error is unavailable. As a result, only the rounding and truncation error can be utilized to discriminate between singly and doubly compressed images with the same quantization matrix. So we only focus on these two kinds of error in the next section.

III. Proposed Approach

In this section, we first analyze the error blocks in JPEG compression. Based on the analysis, we show the statistical differences of the error blocks between singly and doubly compressed images, and then propose a set of features to characterize such differences. Finally, support vector machine (SVM) is adopted to learn the discriminability from the extracted features for detecting double JPEG compression with the same quantization matrix.

A. Analysis of Error Blocks in JPEG Compression

Given a JPEG image, we decompress it into the spatial domain. Then, we can obtain the error image through the procedure as shown in Fig. 1. In this subsection, we first present

[1]It is assumed that JPEG coefficients can be directly accessed by decoding the bitstream of a JPEG file.

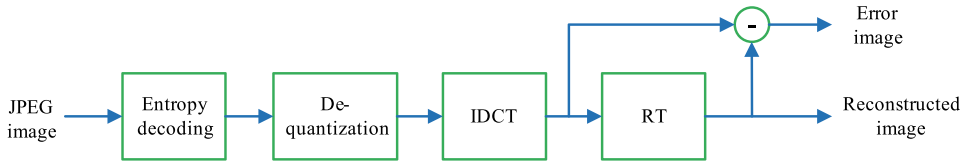

Fig. 1. Flow chart of generating the error image in the JPEG decompression process.

TABLE I
NOTATIONS

$\boldsymbol{K}_n$	JPEG coefficients from a JPEG image file, $\boldsymbol{K}_n \in \mathbb{Z}^{8\times 8}$
$\tilde{\boldsymbol{D}}_n$	de-quantized JPEG coefficients, $\tilde{\boldsymbol{D}}_n \in \mathbb{Z}^{8\times 8}$
$\boldsymbol{R}_n$	error block, $\boldsymbol{R}_n \in \mathbb{R}^{8\times 8}$
$\boldsymbol{F}_n$	DCT coefficients of an error block, $\boldsymbol{F}_n \in \mathbb{R}^{8\times 8}$
$\boldsymbol{M}_n$	quantized DCT coefficients of an error block, $\boldsymbol{M}_n \in \mathbb{Z}^{8\times 8}$
$\boldsymbol{Q}$	quantization matrix, $\boldsymbol{Q} \in \mathbb{N}^{8\times 8}$
$\times$	component-wise multiplication
$/$	component-wise division
RT	rounding and truncation operation

the relationship between error blocks in the two consecutive JPEG compressions/decompressions. The notations used hereinafter are summarized in Table I, where $\mathbb{N}$, $\mathbb{Z}$ and $\mathbb{R}$ denote the sets of natural, integer and real numbers, respectively. The subscript n denotes the times of JPEG compressions an image has undergone.

1) Relationship of Error Blocks Between Two Consecutive Compressions: For the convenience of description, we refer to an image that has been JPEG compressed with the same quantization matrix n times as an n-times compressed image. According to the process that generates the error image in Fig. 1, error blocks of an n-times compressed JPEG image, denoted by $\boldsymbol{R}_n$, can be written as

$$\boldsymbol{R}_n = RT(IDCT(\tilde{\boldsymbol{D}}_n)) - IDCT(\tilde{\boldsymbol{D}}_n) \tag{1}$$

where RT denotes the rounding and truncation operation in JPEG decompression, $IDCT$ denotes the inverse discrete cosine transform, $\tilde{\boldsymbol{D}}_n$ denotes the de-quantized JPEG coefficients during the process of the n-times decompression. According to the definition of de-quantization, we have

$$\tilde{\boldsymbol{D}}_n = \boldsymbol{K}_n \times \boldsymbol{Q} \tag{2}$$

where $\boldsymbol{K}_n$ is the JPEG coefficient matrix of the n-times compressed images, $\boldsymbol{Q}$ is the quantization matrix and the operator "$\times$" represents the component-wise multiplication. Then the relationship between $\boldsymbol{K}_n$ and $\boldsymbol{K}_{n+1}$ can be given by

$$\begin{aligned}\boldsymbol{K}_{n+1} &= [DCT(RT(IDCT(\tilde{\boldsymbol{D}}_n)))/\boldsymbol{Q}] \\ &= [DCT(IDCT(\tilde{\boldsymbol{D}}_n) + \boldsymbol{R}_n)/\boldsymbol{Q}] \\ &= \boldsymbol{K}_n + [DCT(\boldsymbol{R}_n)/\boldsymbol{Q}] \\ &= \boldsymbol{K}_n + \boldsymbol{M}_n\end{aligned} \tag{3}$$

where $[\cdot]$ denotes rounding to the nearest integer, "/" denotes the component-wise division, DCT denotes the discrete cosine transform, and $\boldsymbol{M}_n$ denotes the matrix of quantized DCT coefficients of $\boldsymbol{R}_n$. Based on Eqs. (1), (2) and (3), $\boldsymbol{R}_{n+1}$ can be related to $\boldsymbol{R}_n$ by

$$\begin{aligned}\boldsymbol{R}_{n+1} = \boldsymbol{R}_n &+ RT(IDCT(\tilde{\boldsymbol{D}}_n) + IDCT(\boldsymbol{M}_n \times \boldsymbol{Q})) \\ &- RT(IDCT(\tilde{\boldsymbol{D}}_n)) - IDCT(\boldsymbol{M}_n \times \boldsymbol{Q}).\end{aligned} \tag{4}$$

According to Eq. (4), for an error block $\boldsymbol{R}_n$ in the error image, if $\boldsymbol{M}_n$ is a zero matrix, then $\boldsymbol{R}_{n+1}$ is equal to $\boldsymbol{R}_n$, which means that the error block with $\boldsymbol{M}_n = \boldsymbol{0}$ will no longer change in its next JPEG compression. As done in [17], for an n-times compressed image, we refer to the error blocks with $\boldsymbol{M}_n = \boldsymbol{0}$ as its stable blocks, and refer to those with $\boldsymbol{M}_n \neq \boldsymbol{0}$ as its unstable blocks. Then, based on these definitions, we have the following discussions.

First, as above defined, stable blocks do not change any more, thus only the unstable blocks of an n-times compressed image can provide discriminative information for distinguishing itself from its recompressed version (i.e., the $(n+1)$-times compressed image). Due to this reason, we consider the stable blocks of the n-times compressed image useless and exclude them from the computation of our proposed features. That is to say, when we have a task to distinguish n-times compressed images from $(n+1)$-times compressed images (it is equivalent to the detection of double JPEG compression when $n = 1$), we only need to focus on the error blocks with $\boldsymbol{M}_n \neq \boldsymbol{0}$. For an n-times compressed image, the error blocks with $\boldsymbol{M}_n = \boldsymbol{0}$ can be easily identified and excluded; however, for an $(n+1)$-times compressed image, the blocks with $\boldsymbol{M}_n = \boldsymbol{0}$ are unobservable. Fortunately, the set of the blocks with $\boldsymbol{M}_{n+1} = \boldsymbol{0}$ includes all blocks with $\boldsymbol{M}_n = \boldsymbol{0}$ (this is because if $\boldsymbol{M}_n = \boldsymbol{0}$, as analyzed above, $\boldsymbol{R}_{n+1}$ is equal to $\boldsymbol{R}_n$. Further considering that $\boldsymbol{M}_{n+1} = [DCT(\boldsymbol{R}_{n+1})/\boldsymbol{Q}] = [DCT(\boldsymbol{R}_n)/\boldsymbol{Q}] = \boldsymbol{M}_n$, then $\boldsymbol{M}_{n+1}$ is also a zero matrix). Thus, we adopt $\boldsymbol{M}_{n+1} = \boldsymbol{0}$ instead of $\boldsymbol{M}_n = \boldsymbol{0}$ to identify the useless blocks in an $(n+1)$-times compressed image. Note that the blocks with $\boldsymbol{M}_{n+1} = \boldsymbol{0}$ is just the stable blocks of the $(n+1)$-times compressed image. To summarize, given a JPEG image to be detected, no matter what its compression times is, all its stable blocks are excluded before our feature extraction.

Second, we have analyzed above that if $\boldsymbol{M}_n = \boldsymbol{0}$, then $\boldsymbol{M}_{n+1} = \boldsymbol{0}$, which means that stable blocks are still stable blocks after a new compression, do not change to unstable ones. Therefore, for a given image, the number of unstable blocks can only decrease but not increase with the increase of the times n of JPEG compressions. Furthermore, JPEG compression, which can be viewed as a kind of smooth operation, may cause some unstable blocks to change to stable ones, leading to the number of unstable blocks has a decrease. In general, with the increase of the compression times n, the number of unstable blocks decreases, then it becomes more difficult to distinguish between n-times compressed

images from $(n+1)$-times compressed ones. For example, the discrimination between double and triple compressions is more difficult than that between single and double JPEG compressions.

2) Difference Between Rounding and Truncation Error Blocks: As mentioned in Section II, two kinds of error (i.e., rounding error and truncation error) occur during JPEG decompression. Accordingly, we can categorize error blocks into two classes, i.e., rounding error blocks and truncation error blocks. A rounding error block is a block whose elements all belong to the range $[-0.5, 0.5]$; while a truncation error block is a block of which at least one element exceeds the range $[-0.5, 0.5]$. Let $\boldsymbol{F}_n(u,v)$ denote the (u,v)-th DCT coefficient of an error block $\boldsymbol{R}_n$, where $u,v = 0,\cdots,7$. According to the definition of DCT, we have the following formula

$$\boldsymbol{F}_n(u,v) = DCT(\boldsymbol{R}_n) = \begin{cases} \frac{1}{8}\sum_{i=0}^{7}\sum_{j=0}^{7}\boldsymbol{R}_n(i,j)cos\frac{(2i+1)u\pi}{16}cos\frac{(2j+1)v\pi}{16}, & u,v=0 \\ \frac{1}{4}\sum_{i=0}^{7}\sum_{j=0}^{7}\boldsymbol{R}_n(i,j)cos\frac{(2i+1)u\pi}{16}cos\frac{(2j+1)v\pi}{16}, & \text{otherwise.} \end{cases} \tag{5}$$

If $\boldsymbol{R}_n$ is a rounding error block (denoted by $\boldsymbol{R}_n^r$), then $|\boldsymbol{R}_n^r(i,j)| \le 0.5$, $i,j = 0,1,\cdots,7$. As a result, the absolute value of the direct-current (DC) coefficients, $|\boldsymbol{F}_n^r(0,0)|$, is limited by

$$|\boldsymbol{F}_n^r(0,0)| \le \frac{1}{8}\sum_{i=0}^{7}\sum_{j=0}^{7}|\boldsymbol{R}_n^r(i,j)| \le 4. \tag{6}$$

For the AC coefficients $\boldsymbol{F}_n^r(u,v)$ $((u,v)\neq(0,0))$, similarly we have

$$|\boldsymbol{F}_n^r(u,v)| \le \frac{1}{8}\sum_{i=0}^{7}\sum_{j=0}^{7}|cos\frac{(2i+1)u\pi}{16}cos\frac{(2j+1)v\pi}{16}| \le 8. \tag{7}$$

From Eqs. (6) and (7) we can see that $|\boldsymbol{F}_n^r(u,v)|$ is upper bounded. Note that $\boldsymbol{M}_n = [DCT(\boldsymbol{R}_n)/\boldsymbol{Q}] = [\boldsymbol{F}_n/\boldsymbol{Q}]$. With the increase of quantization steps, it is more and more likely that $[\boldsymbol{F}_n^r/\boldsymbol{Q}] = \boldsymbol{0}$, leading to the decrease of the number of unstable rounding error blocks. If $\boldsymbol{Q}(0,0) > 8$ and $\boldsymbol{Q}(u,v) > 16$ for $(u,v) \neq (0,0)$, then all round error blocks become stable, and thus there are no unstable rounding error blocks available for discrimination. In contrast, truncation error can exceed the range $[-0.5, 0.5]$, so the absolute values of the DCT coefficients of a truncation error block (denoted by $|\boldsymbol{F}_n^t|$) are not constrained by the upper bounds derived above, which means that unstable truncation error blocks can be more resistant to the increase of quantization steps than unstable rounding error blocks. It also implies that the features should be extracted from unstable rounding and truncation error blocks separately due to their intrinsic difference in value range.

According to the above analysis, we summarize two rules to extract effective features for discrimination. First, stable error blocks should be excluded before feature extraction. Second, features should be separately computed from rounding and truncation error blocks.

B. Feature Extraction

In this subsection, we focus on distinguishing between single and double JPEG compressions. We first show the statistical differences between singly and doubly compressed JPEG images, and then propose a set of features for SVM to discriminate between them.

1) Statistical Differences Between Singly and Doubly Compressed Images: To exemplify the statistical differences between single and double JPEG compressions, three image databases are used: the Uncompressed Color Image Database (UCID) [23], the Natural Resources Conservation Service (NRCS) database [24] and the Sun Yat-Sen University (SYSU) database [16]. Note that the SYSU database is the same as "OurLab" database used in [16]. There are 1338 images with size 384×512 or 512×384 in the UCID database, 1542 images cropped with size 512×768 in the NRCS database and 1128 images with size 512×512 in the SYSU database. All these images are converted to grayscale images. Let $max_{i,j}(|\boldsymbol{R}_n^{r,l}(i,j)|)$ and $max_{i,j}(|\boldsymbol{R}_n^{t,s}(i,j)|)$ denote the maximum absolute values of the l^{th} rounding error block and s^{th} truncation error block, respectively. Similarly, let $max_{u,v}(|\boldsymbol{F}_n^{r,l}(u,v)|)$ and $max_{u,v}(|\boldsymbol{F}_n^{t,s}(u,v)|)$ denote the maximum absolute values of DCT coefficients of the l^{th} rounding error block and the s^{th} truncation error block, respectively, where $n = 1,2$, $i,j = 0,1,\cdots,7$, $u,v = 0,1,\cdots,7$. The maximum and average values of $max_{i,j}(|\boldsymbol{R}_n^{r,l}(i,j)|)$ and $max_{i,j}(|\boldsymbol{R}_n^{t,s}(i,j)|)$ are listed in Tables II ($n=1$, single compression) and III ($n=2$, double compression), while those of $max_{u,v}(|\boldsymbol{F}_n^{r,l}(u,v)|)$ and $max_{u,v}(|\boldsymbol{F}_n^{t,s}(u,v)|)$ are listed in Tables IV ($n=1$) and V ($n=2$), respectively. All these statistical values are computed by excluding all stable error blocks.

From Tables II-V, one can observe two facts. First, the error blocks of singly compressed images ($n=1$) exhibit different statistics from those of doubly compressed images ($n=2$) in both spatial and DCT domains. For example, for spatial-domain statistics as shown in Tables II and III, the average value of $max_{i,j}(|\boldsymbol{R}_1^{r,l}(i,j)|)$ and that of $max_{i,j}(|\boldsymbol{R}_2^{r,l}(i,j)|)$ are 0.46 and 0 for the UCID database when QF is 70, respectively. For DCT-domain statistics as shown in Tables IV and V, the average value of $max_{u,v}(|\boldsymbol{F}_1^{t,s}(u,v)|)$ takes 7.32, while that of $max_{u,v}(|\boldsymbol{F}_2^{t,s}(u,v)|)$ takes 6.26.

Second, the statistics of rounding error blocks are considerably different from those of truncation error blocks. It can be seen from Tables II-V that the maximum values of $max_{i,j}(|\boldsymbol{R}_n^{r,l}(i,j)|)$ and $max_{u,v}(|\boldsymbol{F}_n^{r,l}(u,v)|)$ are not larger than 0.5 and 4, respectively. In contrast, the maximum values of $max_{i,j}(|\boldsymbol{R}_n^{t,s}(i,j)|)$ and $max_{u,v}(|\boldsymbol{F}_n^{t,s}(u,v)|)$ are relatively large in most cases. For example, the maximum values of $max_{i,j}(|\boldsymbol{R}_1^{t,s}(i,j)|)$ and $max_{u,v}(|\boldsymbol{F}_1^{t,s}(u,v)|)$ are 37.59 and 30.63, respectively, as shown in Tables II and IV for the SYSU database when QF is 80. Statistical differences also evidently exist between the rounding and truncation error blocks in terms of the average values. It should be specially pointed out that some statistical values of the rounding error blocks

TABLE II

MAXIMUM AND AVERAGE VALUES OF $max_{i,j}(|\boldsymbol{R}_1^{r,l}(i,j)|)$ AND $max_{i,j}(|\boldsymbol{R}_1^{t,s}(i,j)|)$ WITH RESPECT TO BLOCK INDICES "l" AND "s". "r" AND "t" DENOTE THE ROUNDING AND TRUNCATION ERROR BLOCK, RESPECTIVELY

Quality Factor	Maximum value						Average value					
	UCID		NRCS		SYSU		UCID		NRCS		SYSU	
	r	t	r	t	r	t	r	t	r	t	r	t
60	0	60.24	0	49.36	0	70.50	0	17.60	0	13.84	0	21.41
70	0.50	49.10	0.49	47.29	0.48	57.08	0.46	14.37	0.46	11.45	0.47	17.13
80	0.50	38.06	0.50	34.49	0.50	37.59	0.50	10.32	0.50	8.24	0.50	11.95
90	0.50	19.75	0.50	17.29	0.50	20.33	0.44	5.34	0.44	4.34	0.40	6.05

TABLE III

MAXIMUM AND AVERAGE VALUES OF $max_{i,j}(|\boldsymbol{R}_2^{r,l}(i,j)|)$ AND $max_{i,j}(|\boldsymbol{R}_2^{t,s}(i,j)|)$ WITH RESPECT TO BLOCK INDICES "l" AND "s". "r" AND "t" DENOTE THE ROUNDING AND TRUNCATION ERROR BLOCK, RESPECTIVELY

Quality Factor	Maximum value						Average value					
	UCID		NRCS		SYSU		UCID		NRCS		SYSU	
	r	t	r	t	r	t	r	t	r	t	r	t
60	0	50.01	0	41.75	0	57.14	0	17.04	0	14.08	0	19.39
70	0	37.69	0.48	35.02	0	47.40	0	13.64	0.48	11.37	0	15.16
80	0.47	27.54	0.48	25.35	0.39	29.65	0.47	9.48	0.47	7.91	0.38	10.33
90	0.50	14.26	0.50	13.86	0.50	17.08	0.46	4.89	0.46	4.10	0.46	5.19

TABLE IV

MAXIMUM AND AVERAGE VALUES OF $max_{u,v}(|\boldsymbol{F}_1^{r,l}(u,v)|)$ AND $max_{u,v}(|\boldsymbol{F}_1^{t,s}(u,v)|)$ WITH RESPECT TO BLOCK INDICES "l" AND "s". "r" AND "t" DENOTE THE ROUNDING AND TRUNCATION ERROR BLOCK, RESPECTIVELY

Quality Factor	Maximum value						Average value					
	UCID		NRCS		SYSU		UCID		NRCS		SYSU	
	r	t	r	t	r	t	r	t	r	t	r	t
60	0	35.88	0	30.63	0	57.75	0	9.33	0	8.71	0	12.05
70	3.61	33.25	3.39	26.75	3.39	44.50	3.14	7.32	3.11	6.86	3.20	9.64
80	4.00	23.25	4.00	23.00	4.00	30.63	3.94	5.08	3.97	4.82	3.85	6.89
90	4.00	13.63	4.00	13.00	4.00	16.38	1.72	2.59	1.70	2.59	1.62	3.60

TABLE V

MAXIMUM AND AVERAGE VALUES OF $max_{u,v}(|\boldsymbol{F}_2^{r,l}(u,v)|)$ AND $max_{u,v}(|\boldsymbol{F}_2^{t,s}(u,v)|)$ WITH RESPECT TO BLOCK INDICES "l" AND "s". "r" AND "t" DENOTE THE ROUNDING AND TRUNCATION ERROR BLOCK, RESPECTIVELY

Quality Factor	Maximum value						Average value					
	UCID		NRCS		SYSU		UCID		NRCS		SYSU	
	r	t	r	t	r	t	r	t	r	t	r	t
60	0	22.38	0	19.50	0	35.38	0	8.13	0	7.72	0	9.77
70	0	20.63	3.39	16.13	0	26.13	0	6.26	3.39	5.94	0	7.62
80	3.00	13.88	3.00	12.38	2.29	17.63	2.39	4.29	2.53	4.08	2.17	5.28
90	2.58	7.75	2.54	8.50	2.58	8.75	1.72	2.22	1.74	2.17	1.79	2.74

are zeros. This is due to the following reason. When QF is relatively small (such as 60), large steps are applied in coefficient quantization, and unstable rounding error blocks tend to become stable as analyzed in Section III-A.2. Hence, in some cases, there are no unstable rounding error blocks available for computing the statistical values in Tables II-V, resulting in the default value "0". In contrast, unstable truncation error blocks do exist in all of the cases.

In summary, the above two facts imply that rounding and truncation error blocks can provide discriminative information for detecting double JPEG compression, and the two kinds of error blocks show fairly different statistics and thus should be separated for feature extraction.

Apart from the statistics listed in Tables II-V, the numbers of rounding and truncation error blocks between single and double JPEG compressions are also different. Note that rounding error is limited to the range of $[-0.5, 0.5]$ while truncation error can exceed this range. It means that rounding error blocks are likely more fragile to JPEG recompression than truncation error blocks. As a demonstration, for the singly compressed JPEG image with QF = 90 shown in Fig. 2(a), the numbers of rounding and truncation error blocks are 129 and 180, respectively. After recompression with the same QF, there are no rounding error blocks but still 137 truncation error blocks in the corresponding doubly compressed JPEG image shown in Fig. 2(b), indicating that the two kinds of error blocks have different resistance to JPEG recompression. Another comparison with small QF is also given in Fig. 2(c) and (d), where rounding error blocks no longer appear, only leaving truncation error blocks (224 blocks for the singly compressed image and 158 blocks for the doubly compressed image). The above observation indicates that the numbers of rounding and truncation error blocks can be also used for detection of double JPEG compression.

2) Error-Based Statistical Features: We have shown that the error blocks between single and double JPEG compressions

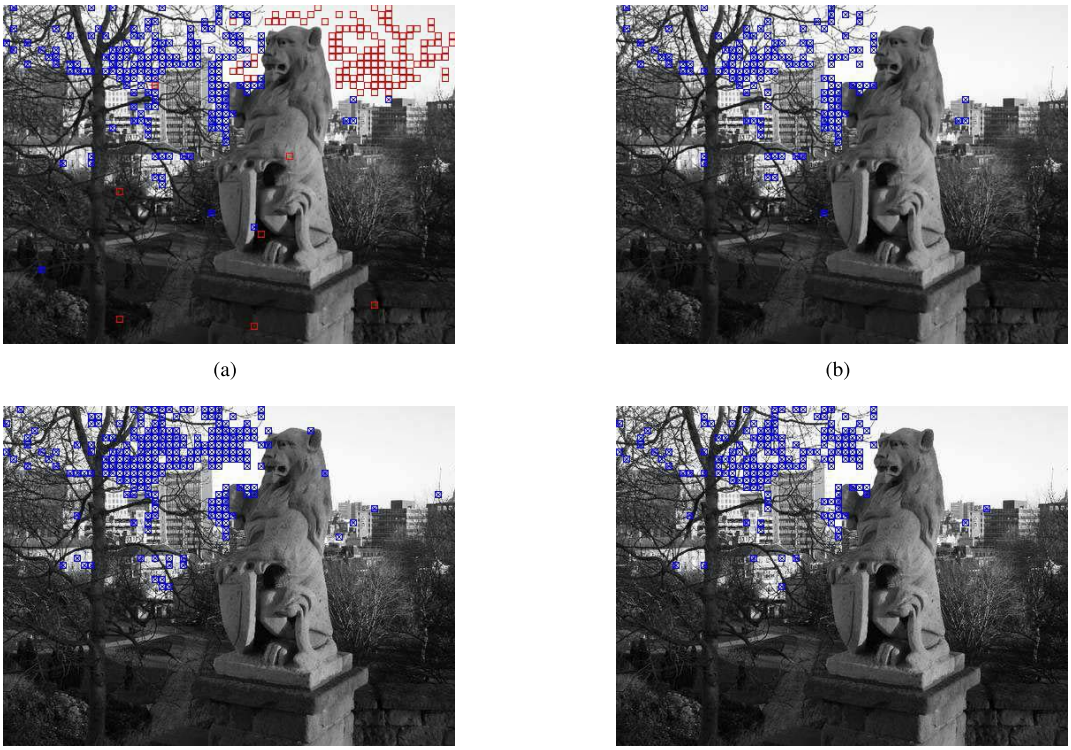

(a) (b) (c) (d)

Fig. 2. Detected rounding and truncation error blocks. (The red block □ and blue block ☒ represent the rounding and truncation error blocks, respectively.) (a) The singly compressed image with QF=90. (b) The doubly compressed image with QF=90. (c) The singly compressed image with QF=70. (d) The doubly compressed image with QF=70.

exhibit different statistical characteristics. In this subsection, the error-based statistical features (EBSF) are extracted from rounding and truncation error blocks separately for detecting double JPEG compression with the same quantization matrix. The EBSF feature set consists of three subsets. The first subset, denoted by EBSF_spatial, is extracted directly from the error image. It contains the means and variances of absolute error values over the rounding and truncation error blocks. For the rounding error blocks, the mean and variance of absolute error values, denoted by $mean(|\boldsymbol{R}_n^r|)$ and $var(|\boldsymbol{R}_n^r|)$, are given by

$$mean(|\boldsymbol{R}_n^r|) = \frac{\sum_{l=1}^{L}\sum_{i=0,j=0}^{i=7,j=7}|\boldsymbol{R}_n^{r,l}(i,j)|}{64L}$$
$$var(|\boldsymbol{R}_n^r|) = \frac{\sum_{l=1}^{L}\sum_{i=0,j=0}^{i=7,j=7}(|\boldsymbol{R}_n^{r,l}(i,j)| - mean(|\boldsymbol{R}_n^r|))^2}{64L} \quad (8)$$

where L denotes the number of the unstable rounding error blocks in the error image. For the truncation error blocks, the mean and variance of absolute error values, denoted by $mean(|\boldsymbol{R}_n^t|)$ and $var(|\boldsymbol{R}_n^t|)$, can also be calculated in a similar way.

Apart from EBSF_spatial, features from the DCT domain of $\boldsymbol{R}_n$, i.e., $\boldsymbol{F}_n = DCT(\boldsymbol{R}_n)$, can also capture statistical differences between single and double JPEG compressions. As a variant of $\boldsymbol{F}_n$, $\boldsymbol{W}_n = [\boldsymbol{F}_n/\boldsymbol{Q}] \times \boldsymbol{Q}$ has been found to be more discriminative. $\boldsymbol{W}_n$ can be viewed as the result of performing JPEG compression on the error image $\boldsymbol{R}_n$ followed by de-quantization. Besides, from Eq. (3), the computation of $\boldsymbol{W}_n$ is equivalent to compressing the reconstructed image again and then calculating the de-quantized JPEG coefficient changes between the two consecutive compressions. The second subset of the proposed features, denoted by EBSF_dct, consists of the means and variances of absolute values of $\boldsymbol{W}_n$ over the rounding and truncation error blocks. It is known that the DC and AC components of DCT coefficients have different characteristics, thus, features from the DC and AC components of $\boldsymbol{W}_n$ should also be extracted separately. For the rounding error blocks, the mean and variance of absolute values of the DC components of $\boldsymbol{W}_n$, denoted by $mean(|\boldsymbol{W}_{n,D}^r|)$ and $var(|\boldsymbol{W}_{n,D}^r|)$, can be given by

$$mean(|\boldsymbol{W}_{n,D}^r|) = \frac{\sum_{l=1}^{L}|\boldsymbol{W}_n^{r,l}(0,0)|}{L}$$
$$var(|\boldsymbol{W}_{n,D}^r|) = \frac{\sum_{l=1}^{L}(|\boldsymbol{W}_n^{r,l}(0,0)| - mean(|\boldsymbol{W}_{n,D}^r|))^2}{L} \quad (9)$$

where $\boldsymbol{W}_n^{r,l}(0,0)$ denotes the DC component of $\boldsymbol{W}_n$ from the l^{th} rounding error block. The mean and variance of absolute values of the AC components of $\boldsymbol{W}_n$, denoted by $mean(|\boldsymbol{W}_{n,A}^r|)$ and $var(|\boldsymbol{W}_{n,A}^r|)$, are

TABLE VI
DETECTION ACCURACY RATES BY EBSF_SPATIAL, EBSF_DCT AND EBSF ON THREE DATABASES

Quality Factor	UCID			NRCS			SYSU		
	EBSF_spatial	EBSF_dct	EBSF	EBSF_spatial	EBSF_dct	EBSF	EBSF_spatial	EBSF_dct	EBSF
95	99.99%	99.66%	100.00%	99.93%	99.76%	100.00%	100.00%	100.00%	100.00%
90	94.65%	95.52%	98.77%	94.78%	95.47%	99.23%	98.40%	97.74%	99.25%
85	92.90%	94.83%	95.57%	92.04%	94.74%	95.18%	82.11%	90.31%	92.07%
80	90.72%	95.10%	95.73%	92.06%	94.76%	95.23%	85.47%	92.98%	94.30%
75	70.67%	82.02%	84.09%	64.78%	75.64%	77.69%	74.59%	85.68%	88.81%
70	65.96%	77.68%	80.81%	63.48%	73.81%	76.27%	71.61%	82.53%	86.64%
60	61.95%	76.00%	78.01%	61.43%	73.57%	76.09%	65.60%	79.09%	85.11%
40	61.90%	74.02%	77.10%	65.33%	72.56%	72.85%	65.10%	76.83%	82.50%
20	66.51%	71.31%	71.40%	63.49%	72.83%	73.34%	67.57%	73.54%	78.20%

$$mean(|\boldsymbol{W}^r_{n,A}|) = \frac{\sum_{l=1}^{L}\sum_{(u,v)\neq(0,0)}|\boldsymbol{W}^{r,l}_n(u,v)|}{63L}$$
$$var(|\boldsymbol{W}^r_{n,A}|) = \frac{\sum_{l=1}^{L}\sum_{(u,v)\neq(0,0)}(|\boldsymbol{W}^{r,l}_n(u,v)| - mean(|\boldsymbol{W}^r_{n,A}|))^2}{63L} \quad (10)$$

where $\boldsymbol{W}^{r,l}_n(u,v)$ $((u,v)\neq(0,0))$ denotes the (u,v)-th AC component of $\boldsymbol{W}_n$ from the l^{th} rounding error block. For the truncation error blocks, the statistical values of the DC and AC components of $\boldsymbol{W}_n$, including $mean(|\boldsymbol{W}^t_{n,D}|)$, $var(|\boldsymbol{W}^t_{n,D}|)$, $mean(|\boldsymbol{W}^t_{n,A}|)$ and $var(|\boldsymbol{W}^t_{n,A}|)$, can also be calculated in a similar way. Note that instead of calculating the means and variances as done in Eq. (10), we can alternatively calculate these statistical values for each of the 63 AC components of $\boldsymbol{W}_n$, which results in a 252-dimensional feature set. The alternative strategy has the advantage of considering the statistical differences among different AC components. However, by our experiments, it can achieve an improvement only in a few cases, at the cost of a significant increase of feature dimensionality. For the simplicity of SVM training, in this paper we prefer to use Eq. (10) to calculate the features of the AC components.

It should be pointed out that both $\boldsymbol{W}_n$ and the feature used in [16] can be computed by performing consecutive JPEG compressions, but they are considerably different. The feature in [16] is the number of different quantized DCT coefficients between two consecutive compressions, whereas $\boldsymbol{W}_n$ is the difference of de-quantized DCT coefficients between two consecutive compressions. Moreover, the method in [16] requires to generate an image-dependent threshold by randomly and slightly modifying some quantized DCT coefficients followed by JPEG compression and decompression multiple times. Whereas, the calculation of $\boldsymbol{W}_n$ does not involve such a process.

The last subset of the proposed features, denoted by EBSF_ratio, contains only one feature. It is the ratio of the number of unstable rounding error blocks, n_r, to the number of all unstable error blocks, n_a, i.e., calculated by n_r/n_a. As mentioned at the end of subsection III-B.1, the ratio n_r/n_a can provide discriminability for detecting double JPEG compression.

In summary, a set of thirteen features, consisting of four features from EBSF_spatial, eight features from EBSF_dct, and one feature from EBSF_ratio, is extracted from each given JPEG image, and the SVM is employed for classification.

IV. EXPERIMENTAL EVALUATIONS

All experiments are conducted on the aforementioned three benchmark databases, i.e., UCID, NRCS and SYSU. All these images are first converted to grayscale images, and singly JPEG compressed with a specific QF to generate negative-class samples. Then the singly compressed images are recompressed with the same QF to generate positive-class samples. For each QF, we randomly choose half of the singly and doubly compressed images as the training samples, and the remaining samples are used for testing. For the classifier, the soft-margin SVM with the Gaussian kernel is employed and the parameters c and γ are determined by a grid-search on the multiplicative grid $(c,\gamma) \in \{(2^i, 2^j)|i \in \{0, 1, \cdots, 20\}, j \in \{-15, -14, \cdots, 3\}\}$. Each training-testing procedure is repeated over 20 times and the average classification accuracy rate is reported.

A. Detection Results on Three Databases

1) Evaluation of Different Subsets of Features: We first evaluate the performance of each individual subset of the proposed features. For the feature EBSF_ratio, when QF is lower than 80, it cannot work well on the three databases. This is because in this case the numbers of rounding error blocks in both single and double JPEG compressions are rather small, which causes no remarkable changes in EBSF_ratio. When QF=80, the detection accuracy rates only with EBSF_ratio on UCID, NRCS and SYSU databases are about 65%, 60% and 62%, respectively. As QF increases, the detection accuracy rates do not increase apparently, which implies that the discriminability of EBSF_ratio is limited. For clarity, Table VI only lists the detection accuracy rates of the other two subsets of features (i.e., EBSF_spatial and EBSF_dct) and the combined features (i.e., EBSF). The investigated QFs are from 20 to 95. Compared to EBSF_ratio, the detection accuracy rates of EBSF_spatial or EBSF_dct on UCID, NRCS and SYSU are much higher. It is also observed from Table VI that in terms of accuracy rate, EBSF_dct is superior to EBSF_spatial when QF is from 20 to 90, while EBSF_spatial outperforms EBSF_dct for QF larger than 90. In addition, from Table VI one can see that the combination of EBSF_ratio, EBSF_spatial and EBSF_dct can improve the detection accuracy rates to an

TABLE VII
EXPERIMENTAL RESULTS BY EBSF WITH THE TPR AND TNR ON THREE DATABASES

Quality Factor	UCID		NRCS		SYSU	
	TPR	TNR	TPR	TNR	TPR	TNR
95	100.00%	100.00%	100.00%	100.00%	100.00%	99.99%
90	98.92%	98.63%	99.24%	99.22%	99.18%	99.31%
85	95.38%	95.76%	95.08%	95.27%	92.08%	92.07%
80	95.31%	96.14%	94.84%	95.62%	94.50%	94.09%
75	84.28%	83.89%	77.98%	77.39%	88.43%	89.19%
70	80.78%	80.85%	77.39%	75.16%	86.29%	86.99%
60	77.42%	78.60%	78.93%	73.25%	84.89%	85.32%
40	78.92%	75.28%	74.59%	71.11%	82.18%	82.81%
20	75.58%	67.21%	72.20%	74.48%	80.04%	76.36%

TABLE VIII
EXPERIMENTAL RESULTS BY EBSF AND HUANG *et al.*'S METHOD [16] ON THREE DATABASES

Quality Factor	UCID		NRCS		SYSU	
	Huang *et al.* [16]	EBSF	Huang *et al.* [16]	EBSF	Huang *et al.* [16]	EBSF
95	99.14%	**100.00%**	99.97%	**100.00%**	100.00%	**100.00%**
90	92.41%	**98.77%**	96.18%	**99.23%**	92.85%	**99.25%**
85	87.89%	**95.57%**	79.75%	**95.18%**	75.98%	**92.07%**
80	85.80%	**95.73%**	78.84%	**95.23%**	76.37%	**94.30%**
75	75.00%	**84.09%**	72.29%	**77.69%**	69.41%	**88.81%**
70	73.65%	**80.81%**	69.21%	**76.27%**	66.40%	**86.64%**
60	—	78.01%	—	76.09%	—	85.11%
40	—	77.10%	—	72.85%	—	82.50%
20	—	71.40%	—	73.34%	—	78.20%

higher level, indicating that each individual subset of features do provide complementary discriminative information.

We also evaluate the EBSF features in terms of true positive rate (TPR) and true negative rate (TNR), as listed in Table VII. Here TPR (TNR) means the ratio of the number of correctly classified doubly (singly) compressed images to the total number of doubly (singly) compressed ones in the test. It is noted that since the numbers of singly and doubly compressed images are equal in our experiments, the detection accuracy rates of EBSF given in Table VI can also be computed as (TPR+TNR)/2. From Table VII, one can see that the TPRs and TNRs are quite balanced for large QFs, while they are a little unbalanced when the QFs are relatively small. Based on our observation, after strong compression there exist considerable images whose both singly and doubly compressed versions do not provide unstable error blocks for feature computation. As a result, the features computed from the singly and doubly compressed images are the same, making them essentially indistinguishable from each other. Therefore, the classifier trained and tested with such features is inevitably biased.

2) *Comparative Evaluation:* Here, we compare our EBSF method with Huang *et al.*'s method [16]. Table VIII shows the detection accuracy rates on the three databases. Since the detection results of Huang *et al.*'s method are not reported in [16] when the QF is 20, 40 and 60, we use symbol '–' to represent these missing results. It is observed that the proposed EBSF method significantly outperforms Huang *et al.*'s method [16] on the three databases with various QFs. Especially on the NRCS and SYSU databases, when the QF is 80 or 85, the gaps between EBSF and Huang *et al.*'s method are up to 15% in detection accuracy rate. For example, when the QF is 80, EBSF can obtain the detection accuracy rates of 95.23% and 94.30% on NRCS and SYSU, which are 16% and 18% higher than those of Huang *et al.*'s method, respectively. Moreover, Huang *et al*. had pointed out that their method becomes considerably unreliable when QF is smaller than 70, and thus did not provide the results for $QF < 70$. In order to obtain a comprehensive evaluation of the proposed EBSF method, the detection accuracy rates for $QF < 70$ are also reported in Table VIII. It can be seen that even when QF is low to 20, the proposed EBSF method can still achieve the detection accuracy rates of up to 70% for the three image databases, indicating that the proposed EBSF method is applicable to a wide range of QFs.

B. Cross Detection Results

To demonstrate the universality of the proposed features, we also conduct cross detection experiments. That is to say, we use the SVM model learned from one of the three image databases to classify the test images from the other two, and the detection accuracy rates are given in Table IX. From the table, we have the following observations. First, the cross detection accuracy rates of our proposed EBSF method are superior to those of Huang *et al.*'s method [16] in most cases. Second, In comparison with Table VIII where the training and testing samples are from the same image database, the detection accuracy rates generally decrease to some extent, which is due to the statistical differences between training and testing samples. However, there also exist some unexpected results. For example, when training and testing both on NRCS at QF 75 (see Table VIII), the accuracy rate is 77.69%, which is lower than that (80.03%) of training on UCID

TABLE IX
CROSS DETECTION RESULTS BY EBSF AND HUANG *et al.*'S METHOD [16] ON THREE DATABASES

Quality Factor	Training samples from UCID				Training samples from NRCS				Training samples from SYSU			
	NRCS		SYSU		UCID		SYSU		UCID		NRCS	
	Huang *et al.* [16]	EBSF	Huang *et al.* [16]	EBSF	Huang *et al.* [16]	EBSF	Huang *et al.* [16]	EBSF	Huang *et al.* [16]	EBSF	Huang *et al.* [16]	EBSF
95	**99.97%**	99.94%	99.96%	**100.00%**	98.99%	**100.00%**	99.91%	**100.00%**	98.62%	**100.00%**	99.81%	**99.97%**
90	95.78%	**98.64%**	92.38%	**93.75%**	91.70%	**99.22%**	90.03%	**93.88%**	91.48%	**97.38%**	95.07%	**97.02%**
85	79.29%	**94.75%**	74.82%	**90.56%**	86.77%	**94.21%**	73.80%	**83.82%**	86.73%	**94.17%**	77.80%	**93.84%**
80	78.54%	**96.17%**	75.93%	**89.18%**	85.54%	**95.03%**	76.11%	**84.80%**	85.20%	**96.04%**	78.48%	**96.30%**
75	72.00%	**80.03%**	68.71%	**81.87%**	74.36%	**76.64%**	69.06%	**73.32%**	74.66%	**85.58%**	71.84%	**81.91%**
70	68.63%	**78.34%**	65.21%	**78.28%**	**73.51%**	72.98%	65.60%	**66.18%**	72.12%	**83.37%**	68.63%	**79.86%**
60	—	76.20%	—	74.78%	—	73.21%	—	61.70%	—	81.35%	—	77.95%
40	—	75.36%	—	72.21%	—	72.46%	—	64.63%	—	79.75%	—	76.59%
20	—	77.76%	—	68.93%	—	68.50%	—	62.72%	—	74.44%	—	77.92%

TABLE X
RESULTS OF DETECTING TRIPLE JPEG COMPRESSION ON UCID BY EBSF AND HUANG *et al.*'S METHOD [16]

Quality Factor	Single-Triple		Double-Triple	
	Huang *et al.* [16]	EBSF	Huang *et al.* [16]	EBSF
95	100.00%	100.00%	99.03%	**99.88%**
90	96.26%	**99.75%**	67.85%	**80.49%**
85	92.89%	**96.91%**	67.12%	**72.62%**
80	91.59%	**96.79%**	66.70%	**70.68%**
75	82.84%	**86.51%**	67.75%	**70.49%**
70	81.39%	**84.05%**	67.08%	**68.67%**

and testing on NRCS. The appearance of such unexpected results can be explained as follows. It is evident that if there exist considerable statistical differences between training and testing samples, then a SVM classifier that is unbiased for the training samples might produce a biased detection result for the testing samples. Furthermore, the balance between TPR and TNR is usually achieved at the cost of accuracy. In other words, an unbiased SVM classifier is probably not the one that achieves the highest accuracy. Therefore, it is possible that an unbiased SVM classifier trained on an image database produces a biased detection result tested on another database, but achieves a higher accuracy. As for the above-mentioned example, when training and testing both on NRCS, the TPR and TNR are 77.98% and 77.39%, respectively, indicating the detection result is well balanced. In contrast, when training on UCID and testing on NRCS, the classifier achieves a higher accuracy, but with an imbalance between TPR (85.60%) and TNR (74.45%).

C. Detection of Triple JPEG Compression

To further explore the potential of the proposed EBSF method, we conduct two experiments to evaluate the discriminability of the EBSF features in detecting triple JPEG compression with the same quantization matrix, which include detection of single-triple JPEG compression and detection of double-triple JPEG compression. In order to make a fair comparison with [16], the same image database, i.e. UCID, is used for evaluation. The comparison results are listed in Table X. One can see that the proposed EBSF method is obviously superior to Huang *et al.*'s method [16] for all tested QFs. In addition, it is interesting to point out that the accuracy rates of detecting single-double compression are higher than those of detecting double-triple compression, but are lower than those of detecting single-triple compression. This is consistent with our knowledge that the difference between single and double JPEG compressions is larger than that between double and triple compressions (which is analyzed in Section III-A.1), while is smaller than that between single and triple compressions.

V. CONCLUSIONS AND DISCUSSIONS

In this paper, we have presented a learning based method to detect double JPEG compression with the same quantization matrix, which is easy to implement while shows promising performance. We first analyzed the error blocks in JPEG compression. Based on the analysis, 13-dimensional error-based statistical features were extracted from rounding and truncation error blocks separately. Finally, with the extracted features, the SVM classifier is applied for detecting double JPEG compression. Experimental results demonstrated that the proposed method is superior to the state-of-the-art method on the UCID, NRCS and SYSU databases with various quality factors.

The differences between the proposed method and Huang *et al.*'s method [16] have two aspects. First, the proposed features can effectively characterize the magnitude information of rounding and truncation error, instead of simply counting the number of different JPEG coefficients as done in [16]. Second, the proposed features are directly extracted from the spatial and DCT domain of the error image, while Huang *et al.*'s method needs to generate an image-dependent threshold by randomly perturbing and JPEG compressing the given image multiple times. It should be pointed out that due to the nonlinearity of rounding/truncation operations and the variety of image statistics, it is still an open problem to make a thorough analysis on the difference of error blocks between two consecutive JPEG compressions with the same quantization matrix.

ACKNOWLEDGMENT

The authors wish to thank the anonymous referees for their valuable comments. They also thank Mr. Changling Tang for his help in the early stage of this work.

REFERENCES

[1] G. K. Wallace, "The JPEG still picture compression standard," *Commun. ACM*, vol. 34, no. 4, pp. 30–44, Apr. 1991.
[2] Z. Fan and R. L. de Queiroz, "Identification of bitmap compression history: JPEG detection and quantizer estimation," *IEEE Trans. Image Process.*, vol. 12, no. 2, pp. 230–235, Feb. 2003.

[3] R. N. Neelamani, R. de Queiroz, Z. Fan, S. Dash, and R. G. Baraniuk, "JPEG compression history estimation for color images," *IEEE Trans. Image Process.*, vol. 15, no. 6, pp. 1365–1378, Jun. 2006.
[4] W. Luo, J. Huang, and G. Qiu, "JPEG error analysis and its applications to digital image forensics," *IEEE Trans. Inf. Forensics Security*, vol. 5, no. 3, pp. 480–491, Sep. 2010.
[5] T. Bianchi and A. Piva, "Image forgery localization via block-grained analysis of JPEG artifacts," *IEEE Trans. Inf. Forensics Security*, vol. 7, no. 3, pp. 1003–1017, Jun. 2012.
[6] H. Farid, "Exposing digital forgeries from JPEG ghosts," *IEEE Trans. Inf. Forensics Security*, vol. 4, no. 1, pp. 154–160, Mar. 2009.
[7] Z. Lin, J. He, X. Tang, and C.-K. Tang, "Fast, automatic and fine-grained tampered JPEG image detection via DCT coefficient analysis," *Pattern Recognit.*, vol. 42, no. 11, pp. 2492–2501, Nov. 2009.
[8] J. Lukáš and J. Fridrich, "Estimation of primary quantization matrix in double compressed JPEG images," in *Proc. Digit. Forensic Res. Workshop*, 2003, pp. 5–8.
[9] A. C. Popescu and H. Farid, "Statistical tools for digital forensics," in *Proc. 6th Int. Workshop Inf. Hiding*, 2004, pp. 128–147.
[10] D. Fu, Y. Q. Shi, and W. Su, "A generalized Benford's law for JPEG coefficients and its applications in image forensics," *Proc. SPIE*, vol. 6505, p. 65051L, Feb. 2007.
[11] B. Li, Y. Q. Shi, and J. Huang, "Detecting doubly compressed JPEG images by using mode based first digit features," in *Proc. IEEE Int. Workshop Multimedia Signal Process.*, Oct. 2008, pp. 730–735.
[12] T. Pevný and J. Fridrich, "Detection of double-compression in JPEG images for applications in steganography," *IEEE Trans. Inf. Forensics Security*, vol. 3, no. 2, pp. 247–258, Jun. 2008.
[13] C. Chen, Y. Q. Shi, and W. Su, "A machine learning based scheme for double JPEG compression detection," in *Proc. 19th Int. Conf. Pattern Recognit.*, Dec. 2008, pp. 1–4.
[14] A. Westfeld, "F5—A steganographic algorithm: High capacity despite better steganalysis," in *Proc. 4th Int. Workshop Inf. Hiding*, 2001, pp. 289–302.
[15] N. Provos, "Defending against statistical steganalysis," in *Proc. 10th USENIX Secur. Symp.*, Aug. 2001, pp. 323–336.
[16] F. Huang, J. Huang, and Y. Q. Shi, "Detecting double JPEG compression with the same quantization matrix," *IEEE Trans. Inf. Forensics Security*, vol. 5, no. 4, pp. 848–856, Dec. 2010.
[17] S. Lai and R. Böhme, "Block convergence in repeated transform coding: JPEG-100 forensics, carbon dating, and tamper detection," in *Proc. IEEE Int. Conf. Acoust., Speech, Signal Process.*, May 2013, pp. 3028–3032.
[18] Y.-L. Chen and C.-T. Hsu, "Detecting recompression of JPEG images via periodicity analysis of compression artifacts for tampering detection," *IEEE Trans. Inf. Forensics Security*, vol. 6, no. 2, pp. 396–406, Jun. 2011.
[19] T. Bianchi and A. Piva, "Detection of nonaligned double JPEG compression based on integer periodicity maps," *IEEE Trans. Inf. Forensics Security*, vol. 7, no. 2, pp. 842–848, Apr. 2012.
[20] W. Luo, Z. Qu, J. Huang, and G. Qiu, "A novel method for detecting cropped and recompressed image block," in *Proc. IEEE ICASSP*, vol. 2. Apr. 2007, pp. 217–220.
[21] L. Wu, X. Kong, B. Wang, and S. Shang, "Image tampering localization via estimating the non-aligned double JPEG compression," *Proc. SPIE*, vol. 8665, p. 86650R, Mar. 2013.
[22] S. Milani, M. Tagliasacchi, and S. Tubaro, "Discriminating multiple JPEG compression using first digit features," in *Proc. IEEE Int. Conf. Acoust., Speech, Signal Process.*, Mar. 2012, pp. 2253–2256.
[23] G. Schaefer and M. Stich, "UCID—An uncompressed colour image database," *Proc. SPIE*, pp. 472–480, Jan. 2004.
[24] *NRCS Photo Gallery*. [Online]. Available: http://photogallery.nrcs.usda.gov, accessed Sep. 1, 2012.

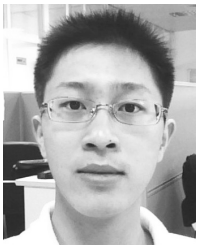

Jianquan Yang received the B.S. and M.S. degrees from Sun Yat-sen University, Guangzhou, China, in 2008 and 2010, respectively. He is currently an Engineer with the Shenzhen Institutes of Advanced Technology, Chinese Academy of Sciences, Shenzhen, China. His research interests mainly include multimedia security and image processing.

Jin Xie received the Ph.D. degree from the Hong Kong Polytechnic University, Hong Kong, in 2012. From 2011 to 2014, he was a visiting student with the Shenzhen Institutes of Advanced Technology, Chinese Academy of Sciences, Shenzhen, China. He is currently a Post-Doctoral Associate with New York University at Abu Dhabi, Abu Dhabi, United Arab Emirates. His research interests include image processing, machine learning, image forensics, computer vision, and graphics.

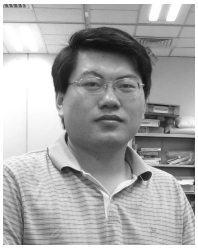

Guopu Zhu (SM'14) received the B.S. degree from Jilin University, Changchun, China, in 2002, and the M.S. and Ph.D. degrees from the Harbin Institute of Technology, Harbin, China, in 2004 and 2007, respectively. He was a Post-Doctoral Fellow with Sun Yat-sen University, Guangzhou, China. He was a Research Associate and Senior Research Associate with the City University of Hong Kong, Hong Kong. Since 2010, he has been an Associate Professor with the Shenzhen Institutes of Advanced Technology, Chinese Academy of Sciences, Shenzhen, China. His main research areas are multimedia security and image processing. He has authored about 20 refereed journal papers in these areas.

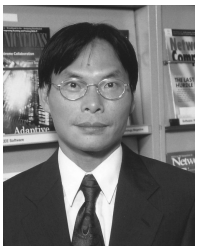

Sam Kwong received the B.Sc. and M.A.Sc. degrees in electrical engineering from the State University of New York at Buffalo, Buffalo, NY, USA, and the University of Waterloo, Waterloo, ON, Canada, in 1983 and 1985, respectively, and the Ph.D. degree from Fernuniversität Hagen, Hagen, Germany, in 1996. From 1985 to 1987, he was a Diagnostic Engineer with Control Data Canada, Mississauga, ON, where he designed the diagnostic software to detect the manufacture faults of the very large scale integration chips in the Cyber 430 machine. He joined Bell Northern Research Canada, Ottawa, ON, as a member of the scientific staff, where he worked on both the DMS-100 voice network and the DPN-100 data network project. In 1990, he joined the City University of Hong Kong, Hong Kong, as a Lecturer with the Department of Electronic Engineering, where he is currently a Professor with the Department of Computer Science. His research interests are in image and video processing, and evolutionary algorithms.

Yun-Qing Shi (F'05) has been with the New Jersey Institute of Technology, Newark, NJ, USA, since 1987. He received the M.S. degree from Shanghai Jiao Tong University, Shanghai, China, and the Ph.D. degree from the University of Pittsburgh, Pittsburgh, PA, USA. His research interests include data hiding, forensics and information assurance, visual signal processing, and communications. He has authored or coauthored over 300 papers, one book, five book chapters, and has edited 10 books. He holds 28 U.S. patents. He was a recipient of the 2010 Innovators Award from the New Jersey Inventors Hall of Fame for Innovations in Digital Forensics and Security. His U.S. patent 7 457 341 entitled "System and Method for Robust Reversible Data Hiding and Data Recovery in the Spatial Domain" received the 2010 Thomas Alva Edison Patent Award from the Research and Development Council of New Jersey. He serves as an Associate Editor of the IEEE TRANSACTIONS ON INFORMATION FORENSICS AND SECURITY, and an Editorial Board Member of a few journals, has served as an Associate Editor of the IEEE TRANSACTIONS ON SIGNAL PROCESSING and the IEEE TRANSACTIONS ON CIRCUITS AND SYSTEMS-II, and served as the Technical Program Chair of IEEE ICME07, the Co-Technical Chair of IWDW, since 2006, and IEEE MMSP05, the Co-General Chair of IEEE MMSP02, and a Distinguished Lecturer of IEEE CASS. He is a member of a few IEEE technical committees.